

2018 Conference on Systems Engineering Research

Exergy Efficiency of Interplanetary Transfer Vehicles

Sean T. Owen^a, Michael D. Watson^{b*}, Mitchell A. Rodriguez^c

^aUniversity of Alabama in Huntsville, Huntsville, AL 35899, USA

^bNASA Marshall Space Flight Center, Huntsville, AL 35812

^cJacobs Space Exploration Group, Huntsville, AL 35806, USA

Abstract

In order to optimize systems, systems engineers require some sort of measure with which to compare vastly different system components. One such measure is system exergy, or the usable system work. Exergy balance analysis models provide a comparison of different system configurations, allowing systems engineers to compare different systems configuration options. This paper presents the exergy efficiency of several Mars transportation system configurations, using data on the interplanetary trajectory, engine performance, and vehicle mass. The importance of the starting and final parking orbits is addressed in the analysis, as well as intermediate hyperbolic escape and entry orbits within Earth and Mars' spheres of influence (SOIs). Propulsion systems analyzed include low-enriched uranium (LEU) nuclear thermal propulsion (NTP), high-enriched uranium (HEU) NTP, LEU methane (CH₄) NTP, and liquid oxygen (LOX)/liquid hydrogen (LH₂) chemical propulsion.

© 2018 The Authors.

Keywords: Interplanetary; Propulsion System; Sphere of Influence; Systems Engineering; System Exergy; Trajectory

1. Introduction

Several space agencies, including NASA, are planning manned exploration of Mars in the upcoming decades. Many different mission architectures have been proposed for accomplishing this. It is the role of systems engineers to compare and optimize different space transportation systems and components, up to and including full mission architectures. To do this, some measure is needed that applies to all systems being compared, even though those systems may have considerable differences. Exergy efficiency, or how well a given system can use the work available to it, provides a measure to compare different interplanetary transfer systems.

* Corresponding author. Tel.: 256-544-3186

E-mail address: Michael.d.watson@nasa.gov

Nomenclature

a	=	semimajor axis
F	=	thrust
f	=	final index
G	=	universal gravitational constant
g_0	=	standard acceleration due to gravity at Earth's surface
h_{prop}	=	enthalpy of the propellant
I_{sp}	=	specific impulse
i	=	initial index
KE	=	kinetic energy
m	=	mass
M_E	=	mass of the Earth
M_{planet}	=	mass of the planet
M_{sun}	=	mass of the sun
m_0	=	initial mass
\dot{m}	=	mass flow rate
$M_{vehicle,initial}$	=	mass of the vehicle on the pad
$M_{vehicle,final}$	=	injected mass
PE	=	potential energy
r	=	distance, position, radius
S	=	positive/negative sign
t	=	time
T_{engine}	=	engine thrust
V	=	velocity
\dot{V}	=	acceleration
V_e	=	exhaust velocity
X	=	system exergy
X_{des}	=	exergy destroyed
X_{exp}	=	exergy expended
η_{exg}	=	exergy efficiency
θ	=	true anomaly
μ	=	gravitational parameter
φ	=	horizon-relative flight angle

2. Exergy Balance Relationship

Planetary transfer vehicles (i.e., satellites, planetary landers, and human and cargo transports as illustrated in Fig. 1) are integrated by system exergy. This includes their propulsion stages, electrical power systems (e.g., nuclear electric or solar electric), and crew volumes for transporting the crew. During propulsive trajectory changes, the exergy balance equation can be written for a spacecraft system as,

$$\sum_{stages} \left[\Delta m_{propellant} \left(h_{prop} + \frac{V_e^2}{2} \right) \right] - X_{des} = \sum_{stages} \left[\left(M_{vehicle,final} \frac{V_{vehicle,final}^2}{2} - M_{vehicle,initial} \frac{V_{vehicle,initial}^2}{2} \right) + \left(\frac{GM_E M_{vehicle,initial}}{r_{altitude,initial}} - \frac{GM_E M_{vehicle,final}}{r_{altitude,final}} \right) \right] \quad (1)$$

The propulsion engine (e.g., chemical, electric, nuclear thermal) characteristics (mass flow, enthalpy, exhaust velocity, and electrical power for electric propulsion) are all included on the left of the equation.

For coast phases of the flight trajectory, the exergy balance equation simplifies to the basic orbital mechanic's relationship for a balanced system. In this case the spacecraft energy (and exergy) is constant and the kinetic and potential energies increase and decrease in opposite directions.



Fig. 1. Mars Transfer Vehicle

$$E_{vehicle} = \left(M_{vehicle} \frac{v_{vehicle}^2}{2} - \frac{GxM_E M_{vehicle}}{r_{altitude}} \right). \quad (2)$$

This creates an oscillatory relationship between the vehicle kinetic and potential energies with respect to the dominate body (typically the sun in interplanetary space).ⁱ

Planetary and solar masses have a large effect on spacecraft exergy in interplanetary space. It is important to ensure an appropriate reference is used. A heliocentric reference is generally best for space travel within the solar system. When operating within a planetary body's sphere of influence (SOI), the sphere in which the planetary gravitational influence is greater than the sun's influence, then the solar influence can usually be ignored. In this case a planetary centric (geospatial reference system for the Earth) can be used. Equation (3), gives the general relationship for the planetary SOI.ⁱⁱ

$$r_{SOI} = r_{sun,planet} \left(\frac{m_{planet}}{m_{sun}} \right)^{2/5} \quad (3)$$

Planetary transfer uses a Hohmann transfer from Earth to Mars and a Hohmann transfer back to Earth. The planetary stay is also important in calculating the possible trajectories. An 11-month stay on the planet is assumed with a total mission length on the order of two to three years. This trajectory contains four main burns: trans-Mars injection (TMI), Mars orbit insertion (MOI), trans-Earth injection (TEI), and Earth orbit insertion (EOI). Four different propulsion systems were analyzed using this basic course: Low enriched uranium (LEU) liquid hydrogen (LH2) nuclear thermal propulsion (NTP), high enriched uranium (HEU) LH2 NTP, LEU CH4 (methane) NTP, and a chemical liquid oxygen (LO2)/LH2 system.

For the LEU CH4 NTP and CHM LOX-LH2 cases, the mass flow rate for the main engine can be calculated from I_{sp} by using Equation (4).

$$\dot{m}_{propellant} = T_{engine} / (I_{sp} g_0) \quad (4)$$

The mass flow rate of the reaction control system (RCS) thrusters is an important parameter in the maneuvers for the trajectory burns. For the calculations in this section, the mass flow rate for a typical RCS thruster of 7 kg/s with an I_{sp} of 291 s will be used.

Fig. 2 shows the exergy efficiency of the LEU LH2 NTP case during the first 500 seconds of TMI, and shows the decline in the efficiency during the RCS burn. Also visible in this plot is an efficiency drop just after the RCS burn; this corresponds to dropping an empty propellant tank. Exergy that was expended to accelerate the tank is lost when the tank is discarded, so dropping the tank registers as a decrease in efficiency.

Exergy calculations are sensitive to changes in position and velocity with respect to the departure and arrival planets, requiring a complete orbital trajectory to calculate exergy efficiency. A patched-conics trajectory is necessary to show the complete system and planetary environments within each planets SOI and in interplanetary space outside the planets SOI's.

3. Orbital Mechanics

For each leg of the mission, the departure planet's and arrival planet's position and velocity are important for the periods when the spacecraft is within the planets SOI.ⁱⁱⁱ Outside the planetary SOI's, the Sun is treated as the sole gravity source. Acceleration due to the

sun's gravity is broken up into vector components along the interplanetary trajectory path. Fig. 3 shows the spacecraft trajectory path and planets orbital paths during the mission.

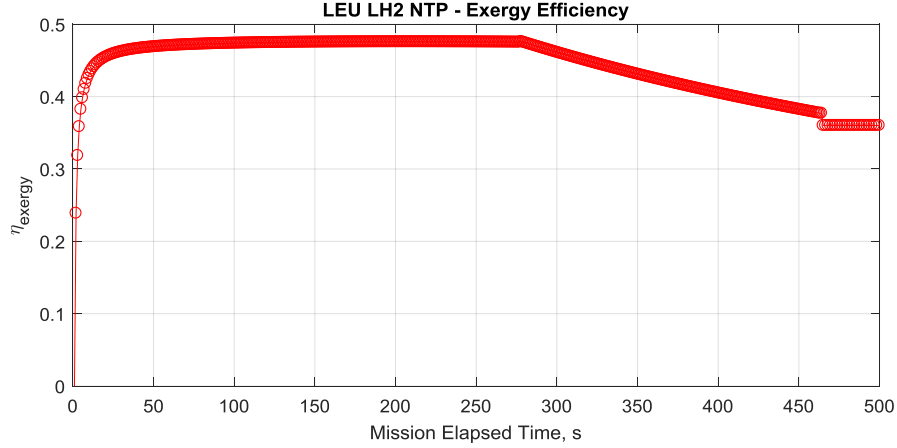


Fig. 2. Exergy efficiency during TMI

Using the planetary positions and the given position of the spacecraft at all points during the mission, the spacecraft's planet-relative distance, speed, and flight angle from the horizon are calculated for the days following the departure burns and leading up to the arrival burns using Equations (5) – (7).

$$\vec{r}_{vehicle,planet} = \vec{r}_{vehicle,sun} - \vec{r}_{planet,sun} \quad (5)$$

$$\vec{V}_{vehicle,planet} = \vec{V}_{vehicle,sun} - \vec{V}_{planet,sun} \quad (6)$$

$$\varphi_{planetary\ horizon} = \frac{\pi}{2} - \text{acos} \left(\frac{\vec{V}_{vehicle,planet} \vec{r}_{vehicle,planet}}{\|\vec{V}_{vehicle,planet}\| \|\vec{r}_{vehicle,planet}\|} \right) \quad (7)$$

Using the spacecraft's distance from the planet over time, the exact time when it crosses the SOI boundary is interpolated with Equation (8). The two points in time used for the interpolation are those just before and after crossing the SOI boundary, the radius of r_{SOI} defined in Equation (3).

$$t_{SOI} = t_i + (t_f - t_i) \frac{r_{SOI} - \|\vec{r}_{vehicle,planet,i}\|}{\|\vec{r}_{vehicle,planet,f}\| - \|\vec{r}_{vehicle,planet,i}\|} \quad (8)$$

With these values, the spacecraft's planet-relative velocity and flight angle from the horizon at that moment are similarly interpolated using Equations (9) and (10).

$$\vec{V}_{vehicle,planet,SOI} = \vec{V}_{vehicle,planet,i} + (t_{SOI} - t_i) \left(\frac{\vec{V}_{vehicle,planet,f} - \vec{V}_{vehicle,planet,i}}{t_f - t_i} \right) \quad (9)$$

$$\varphi_{horizon,SOI} = \varphi_{horizon,i} + (t_{SOI} - t_i) \left(\frac{\varphi_{horizon,f} - \varphi_{horizon,i}}{t_f - t_i} \right) \quad (10)$$

Additionally, a new reference frame is created based on the spacecraft's position and velocity while crossing the SOI boundary, using Equations (11) – (13). Planet-centric orbits within the SOI will be plotted in a 2D plane, and this reference frame will track the orientation of the plane relative to the solar ecliptic.

$$\hat{i} = \frac{\vec{r}_{vehicle,planet,SOI}}{\|\vec{r}_{vehicle,planet,SOI}\|} \quad (11)$$

$$\hat{k} = \frac{ix\vec{V}_{vehicle,planet,SOI}}{\|ix\vec{V}_{vehicle,planet,SOI}\|} \quad (12)$$

$$\hat{j} = \frac{\hat{k}x\hat{i}}{\|\hat{k}x\hat{i}\|} \quad (13)$$

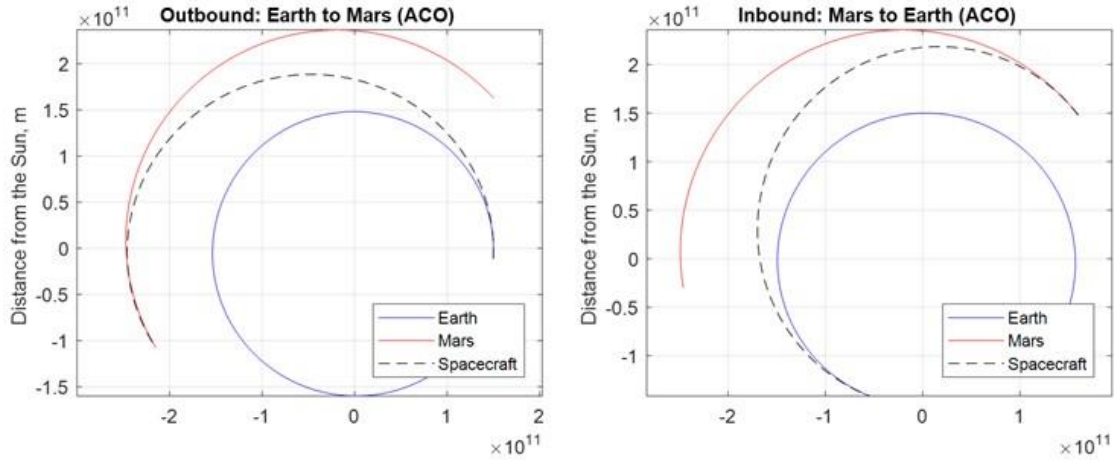


Fig. 3. Spacecraft interplanetary trajectory, and planet trajectories during the outbound and inbound (return) phases

A transformation matrix is created using the new reference frame and Equation (14), and will later be used to convert the SOI orbit back to a heliocentric reference frame.

$$T_{Transform} = \begin{bmatrix} \hat{i}_X & \hat{i}_Y & \hat{i}_Z \\ \hat{j}_X & \hat{j}_Y & \hat{j}_Z \\ \hat{k}_X & \hat{k}_Y & \hat{k}_Z \end{bmatrix} \quad (14)$$

With conditions at the SOI intersection established, the planet-centric transfer and parking orbits within the SOI can be determined. First, the transfer orbit's semi-major axis is calculated using Equations (15) and (16).

$$V_{SOI} = \|\vec{v}_{ship,planet,SOI}\| \quad (15)$$

$$a_{transfer} = 1 / \left(\left(\frac{2}{r_{SOI}} \right) - \left(\frac{V_{SOI}^2}{\mu_{planet}} \right) \right) \quad (16)$$

The speed and flight angle of the spacecraft at the edge of the SOI is sufficient to define a hyperbolic orbit past the planet. The parking orbit periapsis is established (400 km above the planet's surface, roughly the altitude that the ISS orbits at over Earth in this example). This is the minimum shift that still puts the spacecraft's trajectory well above the atmosphere to avoid significant drag. Note, that aerobraking (not addressed here) requires an orbital altitude within the upper atmosphere with sufficient drag to reduce the spacecraft velocity (ΔV) to enter the prescribed parking orbit. Equations (17) – (4.66) are used to determine the apoapsis of the parking orbit for the listed ΔV at that periapsis.

$$e_{transfer} = 1 - \frac{r_{periapsis}}{a_{transfer}} \quad (17)$$

$$V_{periapsis,transfer} = \sqrt{\mu_{planet} \left(\frac{2}{r_{periapsis}} - \frac{1}{a_{transfer}} \right)} \quad (18)$$

$$V_{periapsis,parking} = V_{periapsis,transfer} - \Delta V \quad (19)$$

$$a_{parking} = 1 / \left(\left(\frac{2}{r_{periapsis}} \right) - \left(\frac{V_{periapsis,parking}^2}{\mu_{planet}} \right) \right) \quad (20)$$

$$e_{parking} = 1 - \frac{r_{periapsis,parking}}{a} \quad (21)$$

$$r_{apoapsis} = r_{periapsis} \left(\frac{1+e_{parking}}{1-e_{parking}} \right) \quad (22)$$

It is important for the apoapsis to remain within the planet's SOI and should be established to meet the parking orbit period necessary to meet mission objectives. Once the apoapsis and periapsis are established, the parking orbit periapsis is kept as the periapsis of the hyperbolic transfer orbit. This results in an extremely elliptical parking orbit with a very long period (particularly if it extends to the planetary SOI boundary). Equations (4.61) – (4.66) can be solved iteratively starting with an initial periapsis estimate and stepping in small increments (e.g., 100 mi periapsis altitude increases) until a reasonable apoapsis is found.

The eccentricity of the hyperbolic transfer orbit, the spacecraft's true anomaly at the SOI boundary, and its periapsis velocity can be calculated using Equations (17), (18), and (23).

$$\theta_{SOI} = \arccos \left(\frac{a_{transfer}(1-e_{transfer}^2)-r_{SOI}}{r_{SOI}e_{transfer}} \right) \quad (23)$$

By applying the listed ΔV at the new periapsis as a point-thrust burn, the shape of the parking orbit around the planet can be approximated using Equations (19) – (21). It is only an approximation because it assumes a point-thrust burn connects the transfer and parking orbit. As long as the chosen propulsion system is sufficiently high-thrust, the actual parking orbits will be quite close to the listed values here, as a sufficiently short burn time (on a timescale of minutes) will be negligible compared to the period of the parking orbit.

The parking orbits are only an approximation based on point-thrust burns. In order to properly calculate the exergy efficiency, plots of the spacecraft's position and velocity during each burn will be needed. To do this, Equations (24) and (25) can be used to track the spacecraft forwards or backwards in time from periapsis to establish its trajectory. Another acceleration vector from the spacecraft's engine is added, aimed directly opposite its velocity vector at any point in time for backward tracking. This new vector is split into \hat{i} and \hat{j} components for the calculations.

$$r_f = r_i + V_i \Delta t + \frac{1}{2} \dot{V}_i \Delta t^2 \quad (24)$$

$$V_f = V_i + \dot{V}_i \Delta t \quad (25)$$

At this point, a complete planet-centric course contains the spacecraft's position and velocity from engine start to SOI exit (or vice versa for entry scenarios). This course is then rotated such that the SOI exit/entry point lies directly on the \hat{i} axis of the planet-centric reference frame. Equations (26) and (27) are then used to plot the spacecraft's heliocentric position and velocity while it is inside the SOI.

$$\vec{r}_{vehicle,sun} = \vec{r}_{planet,sun} + (T_{Transform} \vec{r}_{vehicle,planet}) \quad (26)$$

$$\vec{V}_{vehicle,sun} = \vec{V}_{planet,sun} + (T_{Transform} \vec{V}_{vehicle,planet}) \quad (27)$$

4. Interplanetary Exergy Efficiency

With the modified mass data and orbital data in hand, the actual exergy calculations can begin. During each burn of the mission, changes in expended exergy are calculated using Equation (28) which is taken from Equation (1), with mass drops for each time step being calculated from the tank drops and consumable use schedules. These step changes are then summed to produce a plot of expended exergy that rises during burns but otherwise stays constant.

$$X_{exp} = \Delta m_{propellant} \left(h_{prop} + \frac{v_c^2}{2} \right) \quad (28)$$

In order to calculate destroyed exergy, changes in kinetic and potential energy must be tracked across the entire mission. To determine whether the change in kinetic or potential energy should be positive or negative during a given time step, the ruleset described

below in Table 1 is applied, based on Equations (29) and (30). Changes in the spacecraft's velocity and distance relative to the central body during that time step are taken into consideration when determining the sign. It should be noted that the values X, Y, and Z in the table are all greater than or equal to one.

$$KE: m_f V_f^2 - m_i V_i^2 = \begin{cases} > 0 \\ < 0 \end{cases} \quad (29)$$

$$PE: \frac{m_i}{r_i} - \frac{m_f}{r_f} = \begin{cases} > 0 \\ < 0 \end{cases} \quad (30)$$

Table 1. Sign convention for changes in kinetic and potential energy

Mass	Velocity	ΔKE_{step}	Distance	ΔPE_{step}
$M_f = M_i$	$V_f > V_i$	+	$r_f > r_i$	+
$M_f = M_i$	$V_f < V_i$	-	$r_f < r_i$	-
$\begin{cases} M_f > M_i \\ M_f = XM_i \end{cases}$	$\begin{cases} V_f > V_i \\ V_f = ZV_i \end{cases}$	+	$\begin{cases} r_f > r_i \\ r_f = Yr_i \end{cases}$	$\begin{cases} + (Y > X) \\ - (Y < X) \end{cases}$
$\begin{cases} M_f > M_i \\ M_f = XM_i \end{cases}$	$\begin{cases} V_f < V_i \\ V_i = ZV_f \end{cases}$	$\begin{cases} - (Z^2 > X) \\ + (Z^2 < X) \end{cases}$	$\begin{cases} r_f < r_i \\ r_i = Yr_f \end{cases}$	-
$\begin{cases} M_f < M_i \\ M_i = XM_f \end{cases}$	$\begin{cases} V_f > V_i \\ V_f = ZV_i \end{cases}$	$\begin{cases} + (Z^2 > X) \\ - (Z^2 < X) \end{cases}$	$\begin{cases} r_f > r_i \\ r_f = Yr_i \end{cases}$	+
$\begin{cases} M_f < M_i \\ M_i = XM_f \end{cases}$	$\begin{cases} V_f < V_i \\ V_i = ZV_f \end{cases}$	-	$\begin{cases} r_f < r_i \\ r_i = Yr_f \end{cases}$	$\begin{cases} - (Y > X) \\ + (Y < X) \end{cases}$

Change in kinetic and potential energy during a given time step is then calculated using Equations (31) and (32), where S is the sign taken from the previous table, either 1 or -1.

$$\Delta KE_{step} = \frac{S}{2} |m_f V_f^2 - m_i V_i^2| \quad (31)$$

$$\Delta PE_{step} = S\mu \left| \frac{m_i}{r_i} - \frac{m_f}{r_f} \right| \quad (32)$$

These step changes in kinetic and potential energy are summed over time to create a running total of energy changes. These sums are subtracted from the expended exergy using Equation (33) to calculate the exergy destroyed, which then directly leads to the exergy efficiency, defined in Equation (34), at that point in time.

$$X_{des} = X_{exp} - \sum \Delta KE_{step} - \sum \Delta PE_{step} \quad (33)$$

$$\eta_{exergy} = \frac{\Delta m_{propellant} \left(h_{prop} + \frac{V_e^2}{2} \right) - X_{des}}{\Delta m_{propellant} \left(h_{prop} + \frac{V_e^2}{2} \right)} = 1 - \frac{X_{des}}{\Delta m_{propellant} \left(h_{prop} + \frac{V_e^2}{2} \right)} \quad (34)$$

When the spacecraft is within a planet's SOI and not burning propellant, efficiency does not stay constant, but fluctuates with the planetary gravity influences as the vehicle and planet both move along their respective trajectories. This is avoided by using a patched-conics model for the orbital modifications, where exergy calculations are applied to each SOI independently, not using the heliocentric portion of the trajectory. Whenever the spacecraft crosses into or out of a SOI, the most recent value for the total change in kinetic and potential energy is carried over to the next series of calculations. This ensures that exergy efficiency stays constant whenever the spacecraft's mass and velocity are constant, even across SOIs.

The final exergy efficiency plots over the whole mission for each propulsion system are given below in Fig. 4 and 5.

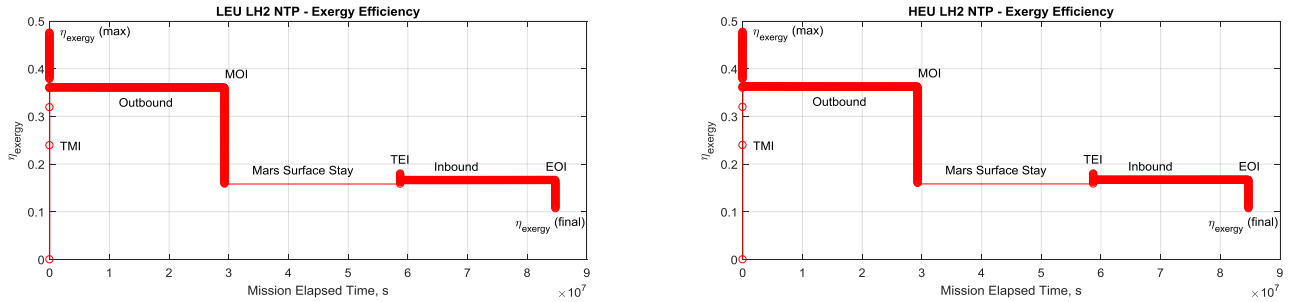


Fig. 4. Exergy efficiency throughout the mission using the LEU LH2 NTP system and the HEU LH2 NTP system.

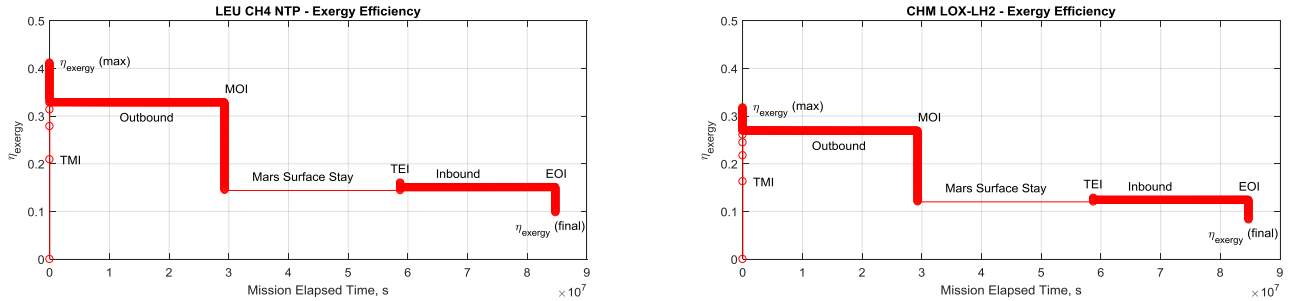


Fig. 5. Exergy efficiency throughout the mission using the LEU CH4 NTP system and the CHM LOX-LH2 system.

As seen previously in Fig. 2, exergy efficiency will sharply rise when using a main engine during a departure burn, and then decrease during the following RCS burn. This is because of the RCS burn’s lower I_{sp} , destroying more exergy for the same exergy expenditure, thus lowering the efficiency of that stage of the mission. Efficiency also drops when ejecting an empty propellant tank or spent consumables, as the exergy expended to move those components up to speed is lost when they are discarded.

Unlike the departure burns, braking burns when arriving at a planet show exergy efficiency decreasing during both the main burn and RCS burn. This is due to how sign conventions for kinetic and potential energy are defined, as well as what equation is being used for exergy efficiency. Both of the definitions used by the program were detailed in the previous section. However, Equation (34) assumes that the vehicle is expending exergy to build up speed. By that definition, any exergy expenditure to shed speed, as in a braking burn, is detrimental to exergy efficiency.

It is possible that different sign conventions for kinetic and potential energy or a different definition of exergy efficiency, used only during braking burns, could show an increase in exergy efficiency during braking. That is future work to investigate the exergy efficiency relationships for braking maneuvers.

Table 2. Final exergy efficiency results for all propulsion systems analyzed.

	LEU LH2 NTP	HEU LH2 NTP	LEU CH4 NTP	CHM LOX-LH2
$\eta_{\text{exg}}(\text{max})$	47.63%	47.68%	41.20%	31.83%
$\eta_{\text{exg}}(\text{total})$	10.61%	10.62%	9.69%	8.18%

Notable efficiency values are given above in Table 2. The maximum exergy efficiency achieved (during the TMI burn) is shown in the top row. The second row shows the total exergy efficiency achieved from the TMI departure burn through parking orbit insertion (EOI) burn at the return to Earth.

Overall, exergy efficiency roughly scales directly with I_{sp} and inversely with the total initial mass of the spacecraft. HEU LH2 NTP achieves the highest efficiencies, but only just barely, since it has the same I_{sp} as the LEU LH2 NTP case and is only minimally lighter due to reactor sizing to produce the same thrust. CHM LOX-LH2 has the lowest efficiencies by far, since its I_{sp} is considerably less than the other cases.

5. Summary

Exergy efficiency provides a mechanism to compare different system options in a clear and effective manner across the full system operational environment. This provides a Measurement of Performance (MoP) for systems engineers to use in comparing very

different system options. This concept has been demonstrated for interplanetary transfer vehicles comparing 4 different system configurations. The result allows a balanced comparison between the options, informing system engineers of the best balanced system to select for the given application. The analysis of interplanetary transfer vehicles shows that NTP options are more efficient than chemical propulsion options, and NTP with liquid hydrogen as a fuel is more efficient than methane as a fuel. This also shows only very small difference between LEU NTP and HEU NTP. This provides key system characterization to support the selection of configuration for interplanetary transfer missions.

References

ⁱ Watson, M. D., “System Exergy: System Integrating Physics of Launch Vehicles and Spacecraft”, AIAA Journal of Spacecraft and Rockets, January 2018.

ⁱⁱ Curtis, Howard, D., “Orbital Mechanics for Engineering Students”, 3rd ed., Elsevier, Boston, 2014.

ⁱⁱⁱ NASA-SP-2009-566, Human Exploration of Mars Design Reference Architecture 5.0, Addendum #2, March 2014.